SPECIAL BOUNDARY CONDITIONS FOR MODELING DIAPHRAGM MOTION AND MITRAL VALVE

João Anderson Isler, joao.isler@usp.br
Bruno Souza Carmo, bruno.carmo@usp.br
Julio Romano Meneghini, jmeneg@usp.br
NDF, Department of Mechanical Engineering, Poli, University of São Paulo, Av. Prof. Mello Moraes, 2231, Cidade Universitária, São Paulo 05508-030, SP, Brazil

Idágene Aparecida Cestari, cestari@incor.usp.br
Bioengineering Division, Heart Institute (InCor), University of São Paulo, Av. Dr. Eneas de Carvalho Aguiar, 44/SS, Cerqueira Cesar, São Paulo 05403-000, SP, Brasil

Abstract. *In this work we took the first steps to create a model to simulate the diaphragm and mitral valve based on special boundary conditions. The pneumatic 35 cc InCor pediatric ventricular assist device (PVAD) was operated at rates of 120 bpm, 90 bpm and 60 bpm with a fixed diastolic duration of 2/3 of the cardiac cycle time to understand the differences of the fluid motion in each condition. However, the mitral and aortic valves were removed from the geometry model. Flow patterns, velocity fields, wall shear rates (WSR) and time-average wall shear rates (TAWSR) were analyzed to evaluate the performance of the device. Our results demonstrate that the model was able to properly represent the three-dimensional WSR on its surface and velocity field inside the device. At high beat rate the PVAD shows excellent performance with acceptable WSR on the device wall, although a very high velocity magnitude was found at the outflow region. However, when the beat rate is reduced, a significant decrease in the WSR occurs, highly increasing the potential of thrombus formation and deposition on the segmented polyurethane, so that the use of the device at reduced beat rate may not be advisable.*

Keywords: *Pediatric ventricular assist device, Artificial heart, Computational fluid mechanics*

1. INTRODUCTION

Ventricular assist devices (VADs) are mechanical circulatory support systems for treatment of end-stage heart failure. They can be used as a heart transplant, bridge to recovery or destination therapy (Hetzer and Stiller, 2006; Pauliks and Ündar, 2008). These devices have been applied for temporary and long-term support, being used as a continuous support in adults for more than five years (Hetzer and Stiller, 2006). These characteristics are extremely important for patients awaiting heart transplantation, especially in case of small children, because of the difficulty of finding a compatible donor (Hetzer and Stiller, 2006). PVADs are confectioned with geometry and materials similar to those employed in adults versions, but in general, present higher rate of hemolysis and thrombus formation, which remains an obstacle to the development of these devices and long-term use.

This report address the growing need for tools to understand the haemodynamic of the 35 cc InCor PVAD under development in the Heart Institute University of Sao Paulo Medical School Hospital for patients under 25 kg of body weight. However, there is a great obstacle to the development for such models, which is the difficulty to simulate the fluid-structure interation (FSI) between the blood and the flexible membranes of the artificial cardiac valves and diaphragm. Hence, firstly, in order to develop a model that properly represents the diaphragm motion and opening and closure of the mitral valve, a preliminary model is presented based on special boundary conditions. In other words, the driving force and the flow direction of the diaphragm are defined by velocity distribution on the diaphragm wall, and the opening and closure of the mitral valve are performed by a velocity waveform which goes to zero in the systolic period.

Previous work by Medvitz et al. (2007) studied a piston motion model based on a physiologic flow waveform observed during experiments and valve closure was modeled by locally increasing the viscosity during the closed phase, which was validated by comparing simulation results with particle image velocimetry (PIV).

2. METHODOLOGY

2.1 Problem description

The pneumatic 35 cc InCor PVAD under development for paracorporeal use is a disposable ventricular orthosis. The pulsatile pump comprises two chambers: pneumatic and sanguine, separated by a medical grade polyurethane flexible diaphragm to act as a blood contacting surface. The blood chamber has changeable volume and contains one inlet and one outlet, in which connectors for cannulas and bovine pericardial valves are accommodated, ensuring a unidirectional flow through the blood chamber and after that to the aorta.

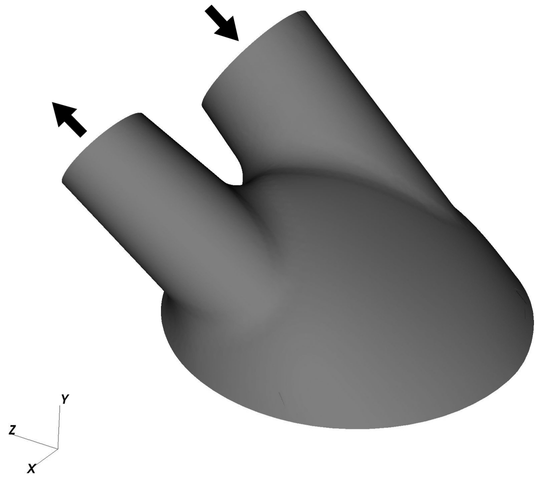

Figure 1. The 35 cc InCor PVAD geometry

The computational simulations of the flow inside the 35 cc InCor PVAD was performed at three different operating conditions. The PVAD was operated at rates of 120 bpm, 90 bpm and 60 bpm to explore the aspects of the fluid motion in each condition. We employed a diastolic duration of 2/3 of the cardiac cycle time for all cases. The mitral and aortic valves were removed, so that there was no obstruction to the flow to get inside the device (Figure 1).

2.2 Computational simulations

An unsteady three-dimensional computational fluid dynamics (CFD) model was developed to assess the performance of the 35 cc InCor PVAD. In this study, blood was treated as an incompressible Newtonian fluid. Numerical simulations were carried out using the Spectral/hp Element Method (Karniadakis and Sherwin, 2005). For the cases investigated in this work, blood is governed by the Navier-Stokes equations. These equations can be written in non-dimensional form as

$$\frac{\partial \mathbf{u}}{\partial t} = -(\mathbf{u}\cdot\nabla)\mathbf{u} - \nabla p + \frac{1}{Re}\nabla^2\mathbf{u}, \tag{1}$$

$$\nabla\cdot\mathbf{u} = 0, \tag{2}$$

where $\mathbf{u} \equiv (u, v, w)$ is the velocity field, t is the time, p is the static pressure and Re is the Reynolds number.

2.3 Diaphragm model

The flexible membrane that separates the pneumatic and sanguine chambers was modeled in a fixed position. Therefore, the diaphragm was dealt by special boundary conditions to represent the diaphragm motion. In other words, the driving force and the flow direction were defined by velocity distribution on the diaphragm wall. The velocity distribution applied on the wall is defined as follows

$$\mathbf{u}_{wall}(x,z,t) = u_{diaphragm}(t)\left(1 - \frac{x^2+z^2}{R_d^2}\right)\hat{\mathbf{y}} \tag{3}$$

where $u_{diaphragm}$(t) is the diaphragm velocity, x and z are the Cartesian coordinates on the plane of the diaphragm with origin in the diaphragm center, R_d is the radius of the region of the diaphragm that is allowed to move and $\hat{\mathbf{y}}$ is the versor component along the y direction.

2.4 Pump cycle

Figure 2 shows velocity waveforms which were applied at the diaphragm and inlet as a function of time and normalized by the mean inlet velocity u_m. From these two waveforms we can easily see the systolic and diastolic periods, in order to simulate the cardiac cycle. Firstly, the diaphragm pushes the blood out of the chamber through the aortic port, while the mitral port remains closed. Afterward, at the diastole, the mitral port is opened and the blood is allowed to enter the chamber and 35 cc is injected within the pump, while the diaphragm velocity is negative. Two important points related to diaphragm negative velocity are noteworthy, in order to justify this modeling. First, in our geometry the diaphragm is a flat surface, however when the diaphragm is in its diastolic position it is curved and can store part of the volume which gets inside the chamber. So, in this way, 20% of the the fluid is taken out of the chamber in the diastole. Second, the force with which the diaphragm pushes the fluid towards itself, when it returns to the diastolic position can be thought as

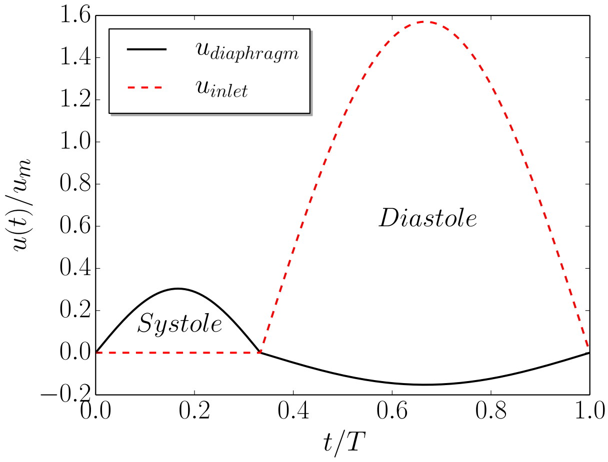

Figure 2. Velocity waveforms applied at the diaphragm and inlet as a function of time.

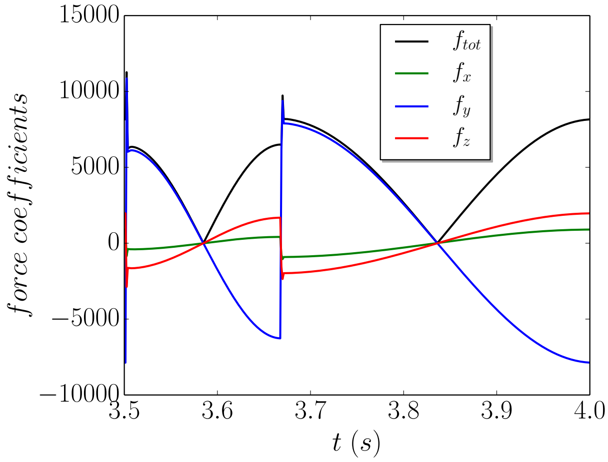

Figure 3. Force coefficients as a function of time when the device is operated at a rate of 120 bpm, using $P = 5$.

a velocity distribution to simulate the suction. The opening and closure of the aortic valve was not modeled, so that the aortic port remains open at the whole cycle. Then, we can define the diaphragm and inlet velocity as follows

$$u_{diaphragm}(t) = \begin{cases} A_{di} sin(\frac{3\pi t}{T}) & \text{if } 0 \leq t/T < \frac{T}{3} \\ A_{do} sin(\frac{3\pi t}{2T} - \frac{\pi}{2}) & \text{if } \frac{T}{3} \leq t/T < T \end{cases} \tag{4}$$

and

$$u_{inlet}(t) = \begin{cases} 0 & \text{if } 0 \leq t/T < \frac{T}{3} \\ A_i sin(\frac{3\pi t}{2T} - \frac{\pi}{2}) & \text{if } \frac{T}{3} \leq t/T < T \end{cases} \tag{5}$$

where $u_{inlet}(t)$ is the inlet velocity, A_{di} is the positive velocity amplitude of the diaphragm, A_{do} is the negative velocity amplitude of the diaphragm and A_i is the inlet velocity amplitude.

2.5 Discretization

The Spectral/*hp* element method was applied to simulate blood flow inside the device, which requires that the computational domain is subdivided into elements. The total number of volume elements constructed for the PVAD was 31355 and all of them are tetrahedrons. Since high-order polynomials can represent the solution within each element of the mesh, the mesh generated in this study was made relatively coarse. The same mesh was used for all simulations even for different operating conditions. Convergence of the solutions was verified calculating the root mean square (RMS) value of the force coefficients on the device surface in the eighth cardiac cycle. The force coefficients as functions of time when the device is operated at a rate of 120 bpm are shown in figure 3. Then the polynomial order, P, was increased within each element to achieve a satisfactory numerical error. The convergence analysis for the three operating conditions are shown

Table 1. The effect of the spectral element polynomial order P on force coefficients at the surface of the PVAD for 120 bpm.

P	fx_{rms}	% difference	fy_{rms}	% difference	fz_{rms}	% difference	ft_{rms}	% difference
6	544.41	–	5153.86	–	1313.79	–	2412.60	–
5	548.54	-0.76	5195.98	-0.81	1324.87	-0.84	2425.86	-0.54
4	552.76	-1.53	5256.52	-1.99	1339.02	-1.92	2487.62	-3.10
3	572.29	-5.12	5419.85	-5.16	1383.59	-5.31	2646.69	-9.70

Table 2. The effect of the spectral element polynomial order P on force coefficients at the surface of the PVAD for 90 bpm.

P	fx_{rms}	% difference	fy_{rms}	% difference	fz_{rms}	% difference	ft_{rms}	% difference
6	409.83	–	3886.28	–	990.60	–	1802.78	–
5	411.04	-0.30	3892.14	-0.15	992.44	-0.19	1819.33	-0.92
4	413.82	-0.97	3933.54	-1.22	1002.01	-1.15	1857.45	-3.03
3	429.28	-4.75	4082.55	-5.05	1041.89	-5.17	2008.04	-11.39

Table 3. The effect of the spectral element polynomial order P on force coefficients at the surface of the PVAD for 60 bpm.

P	fx_{rms}	% difference	fy_{rms}	% difference	fz_{rms}	% difference	ft_{rms}	% difference
5	274.68	–	2605.85	–	664.35	–	1219.28	–
4	276.14	-0.53	2628.85	-0.88	669.63	-0.80	1223.93	-0.38
3	281.94	-2.64	2675.34	-2.66	682.45	-2.72	1305.80	-7.10

Table 4. Comparison of the Reynolds and Strouhal numbers for different operating condition

Operating condition	Re	St
120 bpm	2025	4.2
90 bpm	1519	4.2
60 bpm	1013	4.2

in tables 1, 2 and 3. It can be seen that with 5^{th} order polynomials (i.e. 6^{th} order accuracy in space), which corresponds in terms of degrees of freedom to meshes of approximately 3.9 million tetrahedral elements, the convergence is reached with uncertainty less than 1% in all cases. Hence, the computation simulations were performed using $P = 5$.

The triangular external faces of the tetrahedral elements were curved using SPHERIGON patches (Volino and Magnenat Thalmann, 1998), following a method developed by Plata (2010). Therefore, although the mesh has elements with large sizes the surface mesh is curvilinear.

2.6 Modeling parameters and boundary conditions

The fluid properties were chosen to match the blood analog fluid used in the in vitro experiments. We assume the blood density $\rho = 1099.84\,\mathrm{kg/m^3}$ (Ferrara et al., 2010) and the kinematic viscosity $\nu = 0.03\,\mathrm{cm^2/s}$ (Ferrara et al., 2010). The Reynolds and Strouhal numbers were computed based on the following equations (Bachmann et al., 2000)

$$Re = \left(\frac{4}{\pi\nu}\right)\frac{SV}{D_i}\frac{N}{H} \tag{6}$$

and

$$St = \left(\frac{4}{\pi}\right)\frac{SV}{D_i^3}, \tag{7}$$

where SV is the chamber stroke volume, D_i (= 22 mm) is the diameter of the mitral port, N is the beat rate, H is the ratio of the diastolic time to cycle time and ν is the kinematic viscosity. The values for the Reynolds and Strouhal

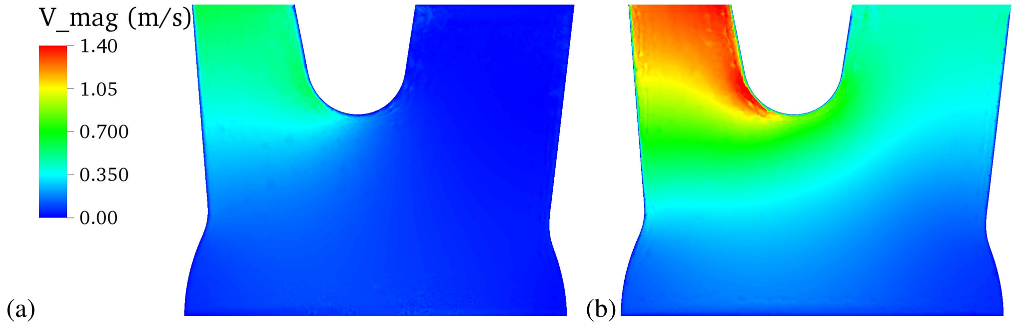

Figure 4. Colour maps of velocity magnitude (m/s) at 120 bpm close to (a) peak systole ($t/T = 0.15$) and (b) peak diastole ($t/T = 0.65$). The slices were taken to 35 degrees from the plane xz.

numbers at the three operating conditions analyzed are showed in table 4. Note that the Strouhal numbers are equal for all cases because it only depends on the geometric parameters. Therefore, regardless of the characteristic length chosen, the Strouhal number will be preserved in geometrically similar pumps. The pressure and the velocity gradient was set up to zero at the outlet boundary condition. A no-slip condition was imposed at the device walls.

2.7 Haemodynamic metric

The TAWSR was calculated using the following definition

$$\text{TAWSR} = \frac{1}{T}\frac{1}{\mu}\int_0^T |\vec{\tau}_w|\, dt \tag{8}$$

where $\vec{\tau}_w$ is the wall shear stress vector and μ is the dynamic viscosity. The TAWSS can be regarded as the time-average of the WSR magnitude.

3. RESULTS AND DISCUSSION

Figure 4 shows the fluid dynamic within the PVAD at operating condition of 120 bpm during a cardiac cycle. At peak systole, when the mitral port was closed and the ejection on the diaphragm is maximum, the fluid is pushed out of the chamber straight to the outflow as shown in figure 4(a). Afterward, at peak diastole, the mitral port was opened and the fluid is ejected inside the chamber, however, in our model the aortic port remains open at the diastole, so that the flow can take two paths. The first of them, the fluid goes directly to the outflow with separated flow at the right wall of the outflow. The second of them, the fluid penetrates more deeply inside the chamber as showed in figure 4(b). This pattern was also observed with steady flow when the mitral and aortic port were opened (Isler et al., 2015). An important aspect to notice about the model is that, during the systolic period the ejection of fluid out of the chamber is not too strong. It mainly occurs because the diastolic volume does not remain inside the chamber so that less fluid is ejected during the systolic period.

Figure 5 illustrates the TAWSR distribution on the PVAD surface at operating conditions of 120 bpm, 90 bpm and 60 bpm, respectively. As we can see the TAWSR pattern becomes increasingly heterogeneous mainly at the outflow region when the beat rate is increased, revealing a strong relationship between beat rate and WSR. Two important observations can be made. The first is that only at 120 bpm the WSR is acceptable at the bottom of the chamber such that it exceeds $500\,\mathrm{s}^{-1}$ at each spatial location for at least a part of the cardiac cycle, allowing a good wall washing pattern, although the TAWSR is lower than $500\,\mathrm{s}^{-1}$ in some regions as shown in figure 5(a). However, there is a high potential of thrombus formation and deposition on the segmented polyurethane due to the low WSR for operating condition of 60 bpm. At any time of the cycle the WSR does not exceed $500\,\mathrm{s}^{-1}$ (Figure 5(c)). The second is that, high WSR is found at the outflow region with peak WSR of the order of $10^4\,\mathrm{s}^{-1}$, nevertheless this is not enough to damage the red blood cells (RBC) if exposed at short times (Deutsch et al., 2006; Sutera and Mehrjandi, 1975). However, attention must be paid in this region because we did not use valves in our model yet, which certainly will increase the WSR in most part of the device due to the strong jets impose by artificial heart valves.

In order to investigate the flow field inside the device in each operating condition the velocity magnitude at the base, inflow and outflow regions, close to the peak diastole ($t/T = 0.65$), are showed in figure 6. It can be seen that the velocity magnitude is low at the bottom of the device in all cases, which explains why the WSR is so low in this region mainly at 60 bpm (Figure 6(a-c)). In addition, there is a drastic fall of velocity inside the device when the beating rate is decreased from 120 bpm to 60 bpm. It should be also noted, that there is a great difference of velocity magnitude and WSR between the inflow and outflow regions which is due to the uneven diameters with peak velocity magnitude of approximately

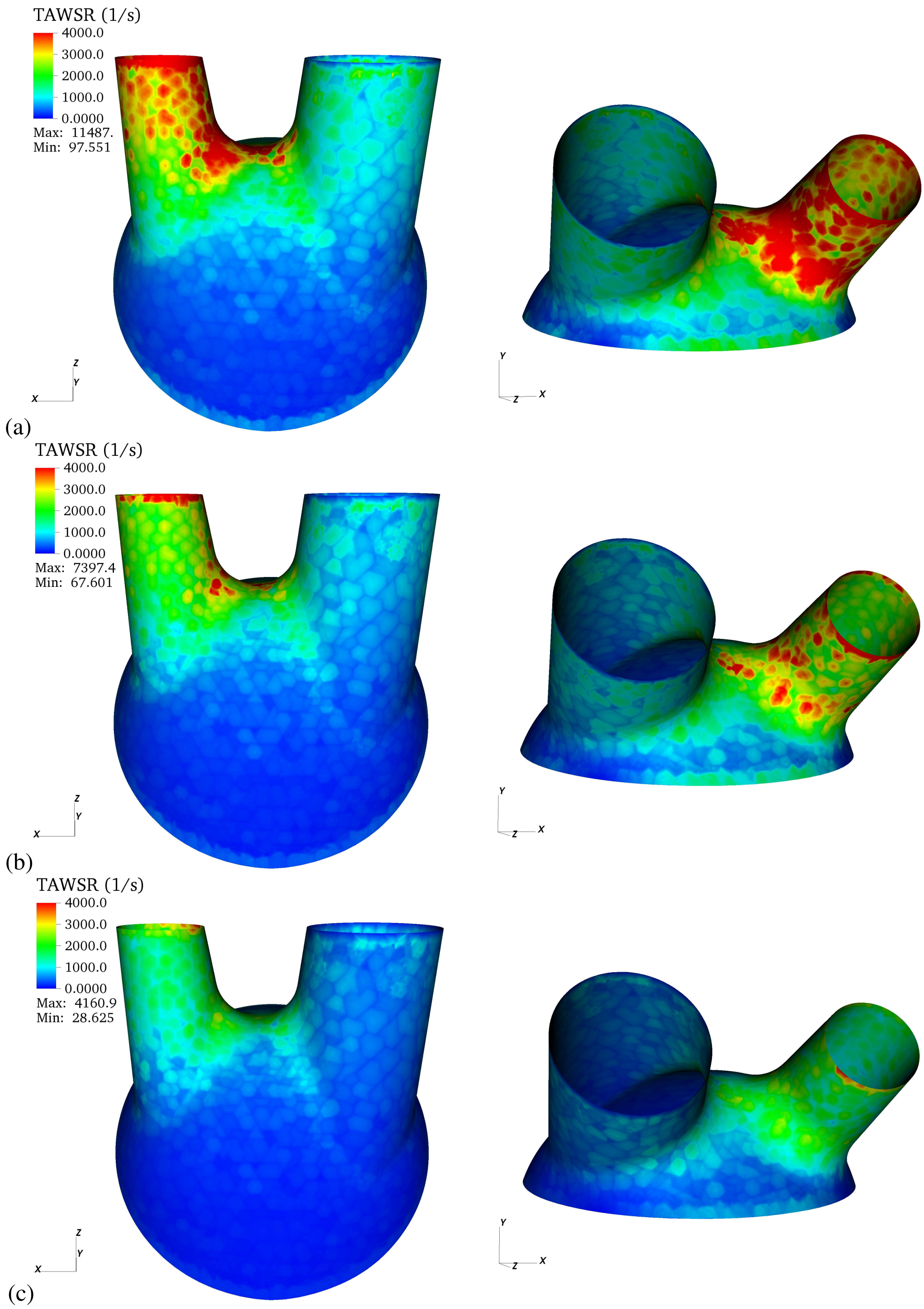

Figure 5. Colour maps of TAWSR (s^{-1}) on the surface of the PVAD at (a) 120 bpm , (b) 90 bpm and (c) 60 bpm.

4.0 m/s at the outflow region at 120 bpm. So the undersized of the aortic port could be prone to high rate of hemolysis. Finally, it is worth mentioning that the vortex formation found close to the inflow region when a steady flow is applied (Isler et al., 2015), was not observed in these simulations. Therefore, the new fluid motion within the PVAD disrupts this pattern.

4. CONCLUSION

Although the preliminary model developed is simple, it was able to properly represent the three-dimensional WSR on its surface and velocity field inside the device which give us an idea of the order of magnitude of these quantities in the prototype. The model still needs to be refined and made more sophisticated, in order to obtain more accurate information to propose changes in the design and improve the hydrodynamic performance of the device.

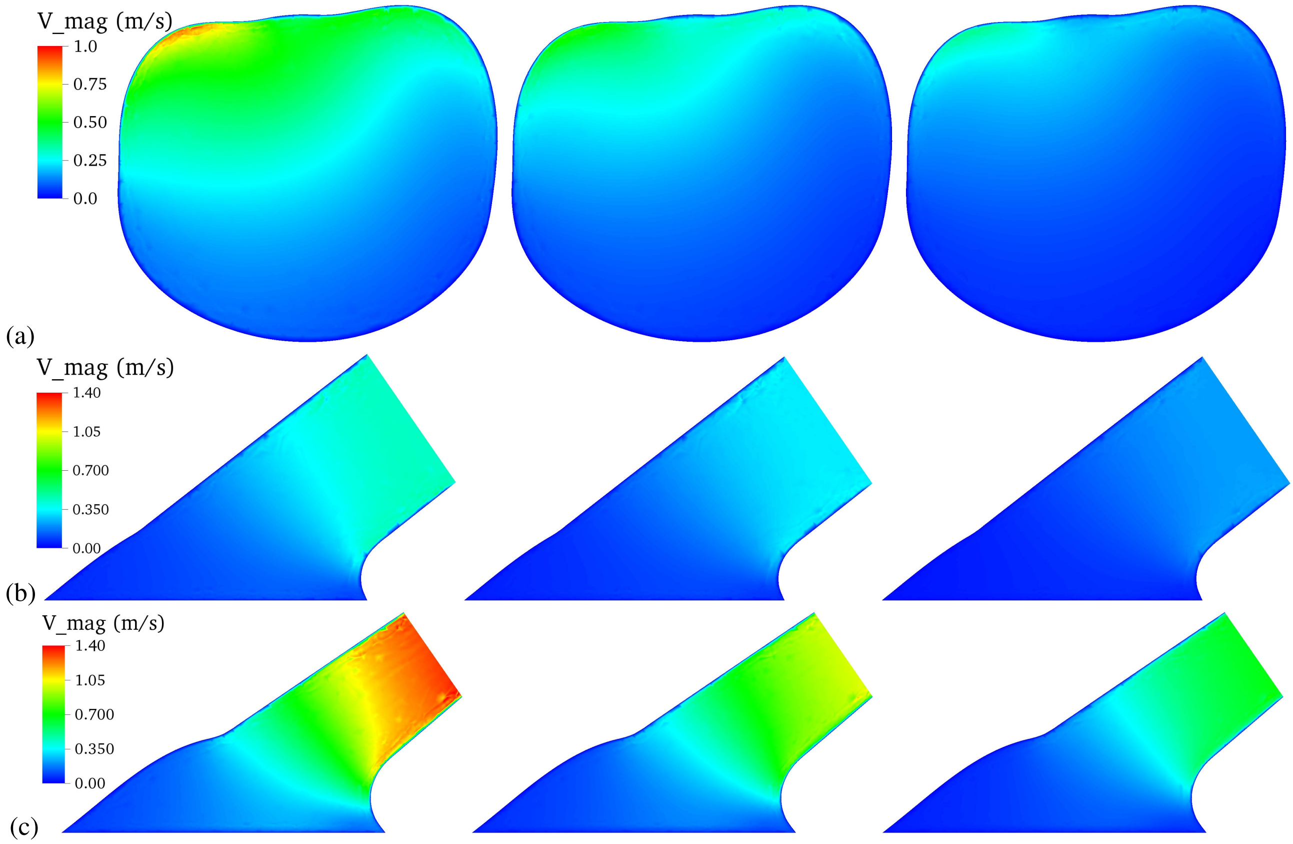

Figure 6. Colour maps of velocity magnitude (m/s) close to the peak diastole ($t/T = 0.65$) at operating condition of 120 bpm, 90 bpm and 60 bpm, respectively from left to right in three different planes. (a) 8 mm from the base face (plane xz), (b) -8 degrees from the plane yz, (c) 8 degrees from the plane yz.

We can conclude, from these first data, that the WSR falls significantly when the beat rate is decreased from 120 bpm to 60 bpm, which can make the use of the device at reduced beat rate not advisable, as also observed in a 15 cc PVAD by Roszelle et al. (2008), owing to the low WSR at the device wall, which has high potential of thrombus formation and deposition on the segmented polyurethane. On the other hand, the PVAD operated at a rate of 120 bpm shows excellent results, so that the WSR is neither high enough to damage the RBC nor low sufficient to allow thrombus deposition. However, it is worth mentioning that the difference between the inflow and outflow diameters causes a great difference of WSR in these two regions, reaching such a value that velocity magnitude achieves approximately 4.0 m/s at the outflow. It should be also noted, that valves were removed, as well as the operating features were not all considered in this model, so that the nature of the fluid dynamic inside the device is not completely represented.

In the future, we will develop a model to close the aortic valve following the approach presented by Avrahami *et al.* (2006a) and Avrahami et al. (2006b), in which the opening and closure are achieved by changes in the fluid viscosity at a region close to the valves. Moreover, a particle tracking model to visualize the flow patterns will be employed to obtain haemodynamics characteristics.

5. ACKNOWLEDGEMENTS

The authors would like to acknowledge the support from FAPESP Project(2012/50283-6). The first author would also like to acknowledge the financial support from CAPES.

6. REFERENCES

Avrahami, I., Rosenfeld, M., Einav, S., 2006a, "The hemodynamics of the berlin pulsatile VAD and the role of its MHV configuration", Annals of Biomedical Engineering, Vol. 34, No. 9, pp. 1373-1388.

Avrahami, I., Rosenfeld, M., Raz, S., Einav, S., 2006b, "Numerical model of flow in a sac-type ventricular assist device", Artificial Organs, Vol. 30, No. 7, pp. 529-538.

Bachmann, C., Hugo, G., Rosenberg, G., Deutsch, S., Fontaine, A.A., Tarbell, J.M., 2000, "Fluid dynamics of a pediatric ventricular assist device", Artificial Organs, Vol.24, No. 5, pp. 362-372.

Deutsch, S., Tarbell, J.M., Manning, K.B., Rosenberg, G., Fontaine, A.A., 2006, "Experimental fluid mechanics of pul-

satile artificial blood pumps", Annual Review of Fluid Mechanics, Vol.38, pp. 65-86.
Ferrara, E., Maramatsu, M., Christensen, K.T., Cestari, I.A., 2010, "Particle-image velocimetry study of a pediatric ventricular assist device", Journal of Biomechanical Engineering, Vol.132, 071004.
Hetzer, R., Stiller, B., 2006, "Technology insight: use of ventricular assist devices in children", Nature Clinical Practice Cardiovascular Medicine, Vol. 3, No. 7, pp. 377-386.
Isler, J.A., Carmo, B.S., Meneghini, J.R., Cestari, I.A., 2015, "Computartional fluid dynamics of a pediatric ventricular assist device", Proceedings of the VI International Conference on Computational Bioengineering, Barcelona, Spain.
Karniadakis, G.E., Sherwin, S.J., 2005, "Spectral/hp Element Methods for Computational Fluid Dynamics", 2nd edn. Oxford University Press, New York, United States.
Medvitz, R.B., Kreider, J.W., Manning, K.B., Fontaine, A.A., Deutsch, S., Paterson, E.G., 2007, "Development and validation of a computational fluid dynamics methodology for simulation of pulsatile left ventricular assist device", ASAIO Journal, Vol.53, pp. 122-131.
Pauliks, L.B., Ündar, A., 2008, "New devices for pediatric mechanical circulatory support", Current Opinion in Cardiology, Vol. 23, pp. 91-96.
Plata, A.M., 2010, Flow and Vascular Nitric Oxide. A computational study of blood flow and vascular nitric oxide transport, Ph.D. thesis, Imperial College London.
Roszelle, B.N., Cooper, B.T., Long, T.C., Deutsch, S., Manning, K.B., 2008, "The 12 cc penn state pulsatile pediatric ventricular ventricular assist device: flow flield observation at a reduced beat rate with application to weaning", ASAIO Journal, Vol.54, pp. 325-331.
Sutera, S.P., Mehrjandi, M.H., 1975, "Deformation and fragmentation of human red blood cells in turbulent shear flow", Biophysical Journal, Vol.15, pp. 1-10.
Volino, P., Magnenat Thalmann, N., 1998, "The spherigon: a simple polygon patch for smoothing quickly your polygonal meshes", Proceedings of Computer Animation, Philadelphia, United States, pp. 72-78.

7. RESPONSIBILITY NOTICE

The author(s) is (are) the only responsible for the printed material included in this paper.